

Nuclear-resonance investigation of the low-mobility region in cubic metallic sodium tungsten bronze, Na_xWO_3 †

D. P. Tunstall*

Laboratory of Atomic and Solid State Physics, Cornell University, Ithaca, New York 14850

(Received 7 October 1974)

Nuclear-resonance measurements of linewidth, Knight shift, nuclear spin-lattice relaxation time T_1 , and spin-echo parameters are reported for ^{23}Na in a series of pseudocubic sodium tungsten bronzes Na_xWO_3 , where x varies from 0.22 up to 0.57. The measurements presented here cover the critical low-mobility region on, and possibly just below, the metallic side of the metal-insulator transition. Structural information on these alloys of low- x value is deduced from x-ray and resonance measurements, arguments are presented for discounting the relevance of percolation theories in understanding the conduction processes in the bronzes of high- x value, the experimental fact that the density of states $g(E_F)$ is directly proportional to x is correlated with recent band-structure calculations, and the strong enhancements of T_1^{-1} in the dilute regime are discussed in the context of the proximity of the metal-insulator transition.

I. INTRODUCTION

This paper presents low-temperature experimental results on the nuclear-resonance parameters, nuclear spin-lattice relaxation time T_1 , spin-spin decay time T_2 , Knight shift K and spin-echo widths, for the sodium nuclei in a series of pseudocubic sodium-tungsten-bronze alloys Na_xWO_3 , with x varying from 0.22 up to 0.57.

The cubic phase of these alloys, which is the stable phase¹ for $x \geq 0.50$ above $T \sim 400$ K, has the perovskite structure, with tungsten atoms at cubic cell corners, oxygen atoms midway along the cube edges, and with sodium sites at the body-centered bc positions (a fraction x of these bc positions are then occupied) (Fig. 1). Below $T \sim 400$ K, for $x \geq 0.50$, Bonera *et al.*¹ have presented NMR evidence that either all or a fraction of the cells become slightly distorted. (Room-temperature x-ray powder diffraction does not show up this distortion.) We label this distorted phase as pseudocubic. All the samples in this study have this phase; those having $x \leq 0.50$ are metastable alloys, formed at high temperature and then rapidly cooled.

The sodium tungsten bronzes can be formed with x values from 0 to 0.9, and it is possible to obtain single crystals having the simple pseudocubic phase over a wide range of x values. At the high- x end of the range, sodium tungsten bronze is an excellent conductor, $\sigma \sim 10^5$ ($\Omega \text{ cm}$)⁻¹ at room temperature [where $\sigma(\text{Cu})$ is 6×10^5 ($\Omega \text{ cm}$)⁻¹]. This conductivity has a metallic temperature dependence, with a high residual resistivity at 4.2 K. On reduction of x the conductivity worsens,² and the temperature dependence flattens off (giving $\sigma_{1,3} \approx \sigma_{300}$ at $x = 0.25$). Hall-coefficient data² indicate $n = x$, where n is the number of conduction electrons per formula unit, for alloys down to $x = 0.25$. With a room-temperature conductivity of about 700 ($\Omega \text{ cm}$)⁻¹ at $x = 0.22$,

the range of x values studied in this work takes the bronzes through the diffusive regime of conduction (the region³ in between the two limits set by a minimum metallic conductivity and the breakdown of any nearly-free-electron treatment of the electronic states).

There are no theoretical band-structure calculations for Na_xWO_3 in the literature; calculations on cubic perovskite KMoO_3 and ReO_3 have, however, been published recently.^{4,5} From the band structure of these related compounds, and the strong similarity in physical properties between them and Na_xWO_3 for high x , it appears that the conduction bands in Na_xWO_3 are formed predominantly from $5d t_{2g}$ atomic-tungsten orbitals and are about 3 eV wide. An assumption of the theoretical analysis is the neglect of potassium $4s$ and $4p$ orbitals in KMoO_3 (and so of sodium $3s$ and $3p$ orbitals in the similar Na_xWO_3 case); the success in explaining experimental results must be accounted a justification of the assumption. As Mattheiss points out,⁴ the observation of de Haas-van Alphen oscillations in $\text{K}_{0.92}\text{MoO}_3$ and in $\text{Na}_{0.93}\text{MoO}_3$, grossly nonstoichiometric compounds, is an argument in favor of a conduction band not involving $4s$, $4p$ ($3s$, $3p$) alkali character. If the conduction band did have such character, then strong scattering would occur at vacant sites, the mean free path would be reduced, and the oscillations would be washed out. NMR data^{6,7} also indicate an absence of alkali character in the conduction-electron wave function at the Fermi surface. The similar transport properties of Na_xWO_3 at high x , $\text{K}_{0.92}\text{MoO}_3$ and ReO_3 (where the bc site is vacant and the extra electron available for conduction comes from the extra valence of the d -metal ion, rather than from doping with an alkali ion) are another supporting argument. The conduction-electron wave functions at the Fermi surface therefore have no sodium character in high- x

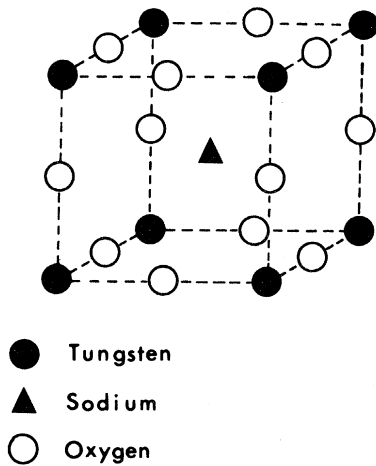


FIG. 1. Cubic cell structure of NaWO_3 .

bronzes. The sodium valence electron apparently goes into the predominantly d conduction band of the host WO_3 . (Pure WO_3 is an insulator or extrinsic semiconductor.^{8,9} Its room-temperature structure is monoclinic.)

The rapid decrease of approximately temperature-independent conductivity as x approaches 0.2 in the sodium tungsten bronzes has generated a lot of comment¹⁰⁻¹²; it is predicted that further experiments on pseudocubic crystals at x values below 0.2 will reveal an insulating state. However, McNeill and Conroy¹³ have reported data on an $x=0.23$ crystal apparently showing a variable-range-hopping type of conduction. At this juncture, it is probable that the transition to a nonmetallic state in the sodium tungsten bronzes, as deduced from transport measurements, occurs at an x value of about 0.24, with $\sigma \sim 10^3$ ($\Omega \text{ cm}$)⁻¹. The transition then has similar characteristics to that in a doped semiconductor,¹⁴ with a smooth decrease of activation energy for the conduction process as the metal is approached from the nonmetallic side. A percolation analysis¹¹ of the x dependence of the conductivity and Hall coefficient in the range down to $x=0.22$ has produced good agreement with experiment. Unfortunately, no experiments have been done on the pseudocubic phase below 0.22, and it may well be impossible to stabilize this phase for lower concentrations. Physically, the alloy system is close to a metal-insulator transition, and the two-phase region¹² of crystal stability close to such transitions may be complicating matters.

In the semiconducting or insulating region of donor doping of tungstic oxide, a region of considerable importance for an understanding of the metal-insulator transition, the experimental data are fragmentary and complicated by various structural phase transitions which modify the electronic trans-

port properties.⁸

Several nuclear-resonance investigations of the sodium-tungsten bronzes have been published.^{1,6,7,15} The most significant features emanating from these studies may be itemized.

(i) In alloys with x values greater than 0.5, the Knight shifts for sodium nuclei are minuscule (~ 50 ppm) and negative.¹⁵

(ii) The spin-lattice relaxation processes in the bronzes, again for $x \geq 0.50$ and sodium nuclei, are metallic in character, in certain temperature ranges, extremely weak, and so consistent with (i).⁶ The data⁶ suggest that the product T_1T is independent of x (where T is the absolute temperature).

(iii) Tungsten nuclear spin-lattice relaxation is metallic in character in the high-density bronzes and efficient.⁷

(iv) Bonera *et al.*¹ explore a phase transition around 400 K, using sodium nuclear resonance. Free-induction-decay rates and spin-lattice relaxation times provide information on this transition in high- x bronzes. The change corresponds to the approximately second-order pseudocubic-to-cubic phase transition and large relaxation enhancements are associated with it. The work¹ emphasizes the presence of two nonequivalent sodium sites in the Na_xWO_3 lattice at low temperature, with the non-cubic fraction of sites being unrelated to x . It is worth remarking that the phase transition, involving considerable displacement of oxygen positions, does not show up in conductivity-against-temperature plots.

Finally, in this brief survey of those properties of the sodium tungsten bronzes that are relevant to an understanding of the work reported in this paper, the specific-heat and magnetic-susceptibility data in the^{16,17} high- x and¹⁸ low- x metallic bronzes indicate that the density of states at the Fermi surface varies linearly with x over a large range.

The sodium-tungsten bronzes in this study therefore are essentially d -metal-oxide metals of simple crystal structure, presumably wide band at high x since the conductivity is so good there (and the lattice parameter *decreases* with decreasing x ¹⁹), exhibiting conductivities in the dilute region that traverse the "diffusive regime" of conduction, and with the most dilute sample having a conductivity quite close to the minimum metallic conductivity.¹¹ The near-perovskite structure at low temperature and the high polarizabilities²⁰ of the base matrix WO_3 make a study of the electronic properties of the sodium-tungsten bronzes near the metal-insulator transition particularly interesting.

In Sec. II the samples used in this study are described and in Sec. III the results are presented. Deductions are made from the results in Sec. IV.

TABLE I. Sample concentrations x in Na_xWO_3 .^a

| Nominal concentration | Chemical concentration | X-ray concentration |
|-----------------------|------------------------|---------------------|
| 0.22 powder | 0.22 | 0.18 |
| 0.25 powder | 0.26 | 0.25 |
| 0.25 crystal | ... | 0.25 |
| 0.30 powder | 0.31 | 0.30 |
| 0.35 crystal | ... | 0.35 |
| 0.35 powder | 0.36 | 0.37 |
| 0.40 powder | 0.40 | 0.42 |
| 0.60 crystal | 0.55 | 0.57 |

^aAn analysis of the width of large-angle scattered x-ray lines indicates an inhomogeneity $\Delta x \sim \pm 0.01$ in these samples.

II. SAMPLES

Eight samples of pseudocubic sodium-tungsten bronze were used in this work. All samples in these NMR experiments were in powder form, made up of irregularly shaped particles of typical dimension $\sim 50 \mu\text{m}$, and were derived²¹ from two master blocks (each about one cubic inch in volume) of bronze grown by electrolysis,² both of nominal composition $\text{Na}_{0.60}\text{WO}_3$. One of these blocks was of very high quality; the other exhibited a less regular shape. X-ray analysis on the high-quality block indicated a good homogeneous single crystal.

To form samples with x value lower than 0.60, diffusion runs² were undertaken on thin slices of the high-quality block lightly packed in a mixture of powders of the lower-quality bronze block with tungstic oxide (WO_3). These runs yield two sources of pseudocubic samples: the diluted slices of single crystal themselves and the resulting host powder. All samples were washed in water and hot NaOH before and after the diffusion runs. For the 0.22, 0.30, and 0.42 samples, the 0.35 powder from the first stage of diffusion was mixed with WO_3 in the first two cases, and with 0.57 powder from the second large block in the third case, and a further stage of diffusion undertaken.

Microprobe analysis of the nominally 0.35 crystal sample indicated homogeneity, within the 20% uncertainty of the technique. Chemical analysis of the crystal samples (i. e., on chips from the slices of crystal used in the diffusion runs) using emission spectroscopy showed Ca present at 100 ppm but nothing else at levels greater than 10 ppm.

Table I, column 3, indicates the results of x-ray analysis of the cubic lattice constant a in the eight samples, taken with the formula¹⁹

$$a = 3.7845 + 0.0820 \text{ \AA}. \quad (1)$$

Column 2, Table I, details the ratio of sodium to tungsten atoms in the samples, as analyzed by atomic absorption spectrometry.

III. RESULTS

The results of these experiments can be classified into three groups of data: T_1 against temperature, Knight shift, and absolute and relative resonance intensities. All results reported here refer to the resonances of the ^{23}Na nuclei in the samples.

Figure 2 details the T_1 measurements plotted against temperature on six of the samples. The Narath-Fromhold data⁶ on an $x=0.89$ sample are also included. The signal used for the measurements in these curves is the free-induction decay (FID) following a $\frac{1}{2}\pi$ pulse, a FID having a decay constant $\sim 500 \mu\text{sec}$. The crystal samples at $x=0.25$ and 0.35 basically duplicated the measurements on the powder samples of the same density, and so that data are not included. Crystal samples were retained for transport property measurements.

T_1 measurements were obtained using a comb sequence to saturate the resonance, followed by a sampling $\frac{1}{2}\pi$ pulse. The T_1 's measured here are long, especially in the more concentrated region.

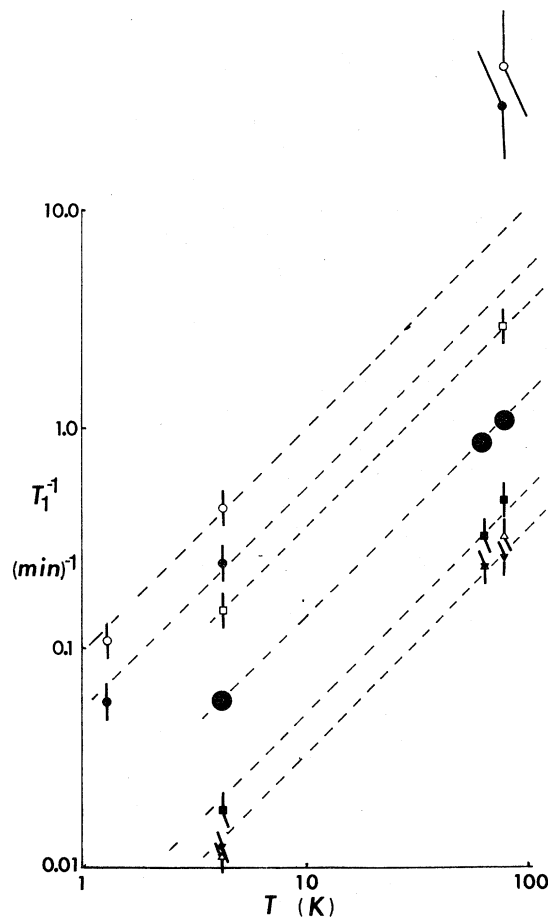


FIG. 2. Plot of T_1 for the ^{23}Na resonance against temperature T for the bronze samples. \bullet 0.89, \blacksquare 0.57, \triangle 0.40, \blacktriangledown 0.35, \square 0.30, \bullet 0.25, \circ 0.22. The dashed lines have a slope +1.

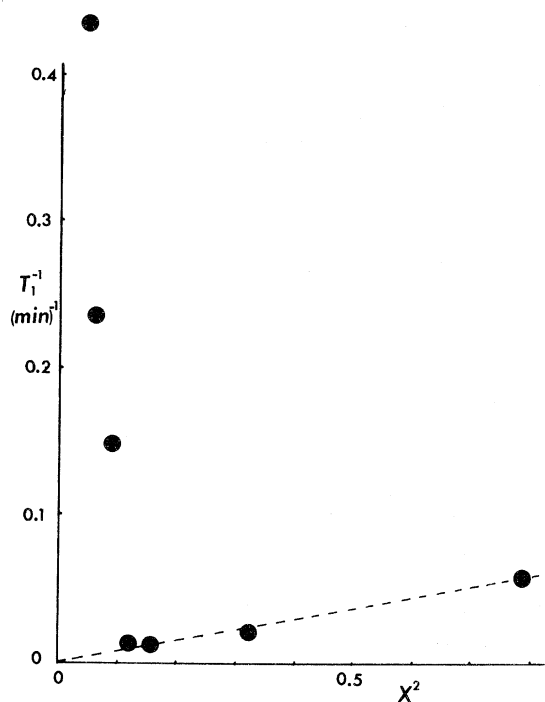


FIG. 3. Plot of the relaxation rate T_1^{-1} at 4.2 K for the Na^{23} resonance against x^2 , including the $x=0.89$ data from Ref. 4.

Because of the extreme length of these relaxation times only enough T_1 determinations were made to decide that, at least at low temperatures, all samples were behaving approximately as $T_1 T = \text{const}$.

A feature of these T_1 results is the nonexponential recovery of magnetization observed in all results for $x=0.30$ and below. The T_1 's for these samples have therefore been defined as the time for the signal to recover to $(1 - e^{-1})M_0$, where M_0 is the signal amplitude at infinite time. This nonexponentiality is apparently not derived from incomplete initial saturation,²² since the results do not change on variation of the comb length (pulses of 100 g and comb parameters of lengths up to seconds and separations ~ 10 msec were used). The shapes of the $(M_0 - M)$ -against-time curves did not change shape with temperature and could be typically changed into pure exponentials by the subtraction of a constant amplitude ~ 10 –20% of M_0 . The line on which the observations were being made was narrow.⁶ It is certainly easily saturated at $x=0.35$ and above, since pure exponential recoveries were observed there with short comb lengths.

A more probable explanation of the nonexponentialities in the dilute samples lies in the deduction made earlier from the x-ray data that small spreads of x occur within any one sample, due probably to less than perfect mixing of the starting powders in the diffusion runs. The rapid variation of T_1 with

x from sample to sample shown in Fig. 2 is manifested within a given sample by nonexponentialities. Examination of the x-ray linewidths, the data in Fig. 2, and the observed nonexponentialities shows them to be consistent with the above model of the origin of the nonexponentialities.

In Fig. 3 the value of T_1^{-1} at 4.2 K is plotted against x^2 . An attempt to see the signal from a noncubic (probably tetragonal) $x=0.1$ sample at this temperature was unsuccessful. This result implies either that $T_1 \approx \infty$ or there is a complete wipeout of the observable resonance due to quadrupole or magnetic interactions; the former explanation is probably correct, since a cw signal was observed in this sample at room temperature (with approximately zero shift). In Fig. 4 the data of Weinberger²³ and Narath and Fromhold⁷ for ^{183}W relaxation are plotted against x^2 for comparison. This latter set of data is taken on high- x bronzes; it is included here to illustrate that the x^2 dependence of T_1^{-1} for ^{23}Na exhibited in the dilute samples above $x \sim 0.35$ is continued into the high- x range, at least in another nucleus. It also illustrates the extreme difference in the relaxation rates for ^{23}Na and ^{183}W . The Knight-shift results are laid out in Table II. Some room-temperature and some 4.2-K results were obtained, the latter being referred to ^{23}Na resonance in sodium metal (a small amount of sodium metal was included within the coil). The room-temperature data were obtained using cw methods on a Varian WL-210 conversion to an E-12 spectrometer²⁴ at 8.5 MHz using NaCl solution as reference. The helium-temperature results were obtained using a wide gate on a box-car integrator to integrate²⁵ the FID after a $\frac{1}{2}\pi$ pulse. The large error bars on the numbers in Table II are a direct result of the extreme smallness of the shifts. If we take the measured shift in sodium metal,²⁶ $K_{\text{metal}} = 1085 \pm 1$ ppm, measured relative to the resonance in sodium metal when the electron spin susceptibility is maintained at zero by microwave irradiation then, relative to the same reference, the shifts in the bronzes at low temperature are seen to be ~ -80 ppm. Both at low and room temperatures the shifts are negative, very small, and consistent with a dependence on x of x^0 or x^1 ; more rapid variations of K with x are excluded by these data. (No importance is attached to the difference between the low- and high-temperature results; the different reference resonances and a small systematic shift in the low-temperature results could account for these effects.) The results are consistent with those of Ref. 15, which resulted from room-temperature measurements.

The intensity of the long FID varies from alloy to alloy as x changes. Two mechanisms that could be contributing to this effect are (a) the obvious linear decrease as the number of sodium atoms is

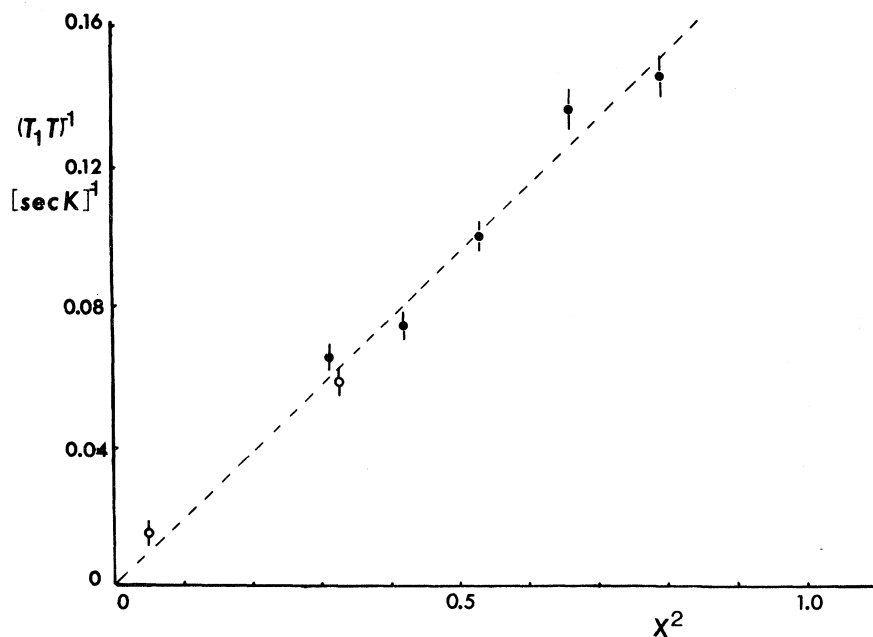


FIG. 4. Plot of the relaxation rate $(T_1 T)^{-1}$ for W^{183} against x^2 , from the tabulated data of Ref. 5, and the data of Weinberg Ref. 23.

reduced, and (b) a breakup of cubic symmetry, due to the reduction of x , a consequent increase in electric field gradients at sodium nuclear sites, and so a first- or second-order quadrupole smearing, or even wipeout,²⁷ of the sodium nuclear resonance. Mechanism (b) is superimposed on (a) and so, if (b) is present, a rapid variation of the FID amplitude with x is predicted. Narath and Fromhold⁶ in high- x samples find that indeed mechanism (b) is present, but that the x dependence generated by it is so weak that they are led to suppose the existence of strong clustering effects in the alloys. Bonera *et al.*¹ suggest that the second mechanism is very weak in their high-temperature nuclear-resonance investigation on alloys with $x \geq 0.52$.

Table III lists the data on intensities obtained from the present study in column 5. This column of results can only be regarded as approximate; it is notoriously difficult to compare intensities of samples accurately, especially powdered metallic samples where different particle sizes in the powder can lead to different packing fractions in the nuclear-resonance sample and to different penetration depths of the rf power. Column 5 indicates that the FID intensity is roughly proportional to x . Mechanism (b) above must therefore be weak. The other columns in Table III refer to various other parameters which impinge upon a discussion of the intensity variation of sodium resonances as a function of x in the tungsten bronzes. None of these parameters is strongly dependent on x ; in fact, only columns 3 and 4 show any systematic variation, with the echo decay time T_2 decreasing as x increases and its width increasing as x increases, down the column.

The data suggest that the FID in bronzes has a time constant $\sim 500 \mu\text{sec}$ independent of x in the range 0.22–0.57. As x decreases the density of magnetically interacting nuclei decreases (dipolar broadening Na-Na dominates the ^{23}Na resonance width¹⁵). In this range of x , a \sqrt{x} dependence of T_2^{-1} on x is expected,²⁸ so that the independence of T_2 (FID) on x is surprising. Quadrupolar effects may be increasing as x decreases in such a way as to counterbalance the reduced dipolar dephasing effects.

Columns 3, 4, and 6 relate to the properties of the echo signal. As noted by Narath and Fromhold,⁶ a two-pulse sequence, $\frac{1}{2}\pi - \pi$, produces a quite different signal from the FID, spaced from the π pulse by a time interval equal to that between the $\frac{1}{2}\pi$ and π pulses. This is the echo (ECHO).

The decay of the ECHO, with time constant given

TABLE II. Knight shifts for ^{23}Na .

| x | Temp (K) | K (ppm) ^a |
|--------------|----------|------------------------|
| 0.22 powder | 4.2 | -1150 ± 20 |
| 0.25 powder | 4.2 | -1150 ± 10 |
| 0.25 powder | 300 | -26 ± 10 |
| 0.35 powder | 4.2 | -1190 ± 30 |
| 0.35 powder | 300 | -26 ± 10 |
| 0.57 crystal | 4.2 | -1180 ± 10 |
| 0.57 crystal | 300 | -45 ± 15 |

^aData taken at 4.2 K were done at 11 MHz and refer to line displacements between ^{23}Na resonance in the bronzes and ^{23}Na resonance in sodium metal. At 300 K, the line displacements involved are those of ^{23}Na resonance in the bronzes and ^{23}Na resonance in a sodium-chloride solution. The frequency was 8.5 MHz.

TABLE III. T_2 and intensity data.

| x | T_2 FID 77 K (μ sec) | T_2 ECHO 4.2 K (msec) | Width ECHO 4.2 K (μ sec) | FID Intensity 77 K (arbitrary units) ^b | Relative intensities ^a Y^c |
|--------------|--------------------------------|----------------------------|----------------------------------|--|--|
| 0.22 powder | 460 | 1.4 | 7 | 1.8 | 47% |
| 0.25 powder | 500 | 1.35 | 10 | 1.4 | 38% |
| 0.30 powder | 560 | 1.5 | 12 | 2.8 | 50% |
| 0.35 powder | 430 | 1.12 | 10 | 3.8 | 42% |
| 0.40 powder | 510 | 1.10 | 13 | 4.4 | 50% |
| 0.57 crystal | 510 | 1.00 | 15 | 4.4 | 43% |

^aThe echo amplitude used in computing this parameter Y is that of the narrow echo; there is in general a much broader and smaller base to the echoes which has been ignored. The presence of this broader echo indicates that the simple partition of the resonance response into two signals may be slightly in error.

^bData on FID amplitudes were taken at a point at least 100 μ sec after the start $\frac{1}{2}\pi$ pulse triggering the FID. This point was also used for T_1 measurements shown in Fig. 1.

^c Y is defined as FID intensity at zero time divided by the sum of the FID intensity at zero time and the extrapolated echo amplitude at zero time.

by column 3, Table III, is again caused by dipolar interactions. The correlation (with opposite slope versus x) of data in columns 3 and 4 makes sense if one assumes that the x dependence of echo width is caused by a variation of second-order quadrupole interactions due to the change of occupancy of nearest-neighbor sodium shells; the decrease in T_2 as x increases, column 3, is then due to an increase of dipolar interaction due to the same change of sodium occupancy. The ratio of T_2 for 0.22 and 0.57 samples assuming dipolar interactions should be $\sim (0.57/0.22)^{1/2} = 1.6$, an x dependence already invoked in discussing the data in column 2.

It seems also necessary to suppose, given the data on echo widths, T_2 (FID) and T_2 (ECHO) in Table III, that the two sorts of signals, FID and ECHO, originate from sodium nuclei in different crystalline environments. Clearly, the contributing nuclei to the FID are situated in a predominantly cubic environment (although cubic symmetry is possibly distorted sufficiently to remove satellites $\pm \frac{1}{2} \leftrightarrow \pm \frac{3}{2}$ transitions from the resonance). In a cubic $\text{Li}_{0.35}\text{WO}_3$ crystal, Lightsey² finds distinct satellites at ± 12 G in cw nuclear resonance on Li⁷. The cw lines obtained in measuring the Knight shifts of Table II showed much less accentuated structure, but satellites were probably visible, at fields $\sim \pm 1$ G. Rather more than half (column 6 Table III) of the sodium nuclei must be associated with a heavily distorted crystalline environment, an environment quite sensitive to sodium occupancy of nearest-neighbor sodium shells (column 4, Table III). For these nuclei all satellite transitions are unobserved; the central line itself $\pm \frac{1}{2} \leftrightarrow \pm \frac{1}{2}$ is heavily broadened by second-order effects. The ECHO nuclei probably outnumber FID nuclei by two or three to one.

A central question now emerges: If the FID and ECHO nuclei are close neighbors to each other,

how will their decay times be affected? In particular, why is T_2 (FID) only of the order of one-half T_2 (ECHO)? Taking the known linewidth¹⁵ in an $x = 0.89$ sample of 1.11 Oe and assuming a Gaussian shape, then a decay T_2 of 400 μ sec is predicted; applying the known functional dependence on $x(x^{-1/2})$, the $x = 0.57$ sample should have $T_2 \approx 500$ μ sec and the $x = 0.22$ sample a T_2 of 810 μ sec. The experimental T_2 (FID) values are shortened below these theoretical figures by only slight broadening of the cw linewidth from quadrupolar effects; at the same time the T_2 (ECHO) values are lengthened above these figures because only the central $\pm \frac{1}{2} \leftrightarrow \pm \frac{1}{2}$ transition is observed. The effects of quadrupolar interactions on T_2 have been summarized by Abragam.²⁹ In the case, for example, where adjacent nuclear dipoles have their $m_s = \pm \frac{1}{2} \leftrightarrow \pm \frac{1}{2}$ transitions occurring at different frequencies, a case which arises when second-order quadrupole interactions vary from site to site, then the nuclei become effectively "unlike" in the context of their dipolar interactions, and their T_2 is extended by $\sim 50\%$.

It seems then that the linewidth, T_2 (FID), T_2 (ECHO), and intensity data coming out of this nuclear resonance study of low- x pseudocubic bronzes are consistent with a simple model. The model supposes first that a fraction, approximately one-third or one-quarter of ²³Na nuclei, are in crystalline sites with cubic symmetry, the rest being in heavily distorted sites. In a crystal where quadrupole interactions were generated solely by this crystal symmetry effect, two signals would be predicted (i.e., a FID and an ECHO), but with both having characteristic T_2 decays longer than in the absence of quadrupole effects. In the model crystal, however, the introduction of quadrupolar interactions generated by the random positioning of ²³Na nuclei would reduce the T_2 of the FID and perhaps also elongate the already long T_2 of the ECHO.

IV. DISCUSSION

The salient features that emerge from Sec. III may be listed.

(i) For each alloy the particular product (T_1T) stays roughly constant at least at low temperatures. So metallic-type relaxation via hyperfine interactions with a degenerate sea of Fermi electrons appears to be the mechanism for transfer of nuclear spin energy to the lattice.

(ii) The same interaction mechanism accounts for the very small Knight shifts, since K and T_1T are related approximately by $K^2T_1T = (\hbar/4\pi k)(\gamma_e/\gamma_n)^2$, the standard Korringa³⁰ product, for samples with $x \geq 0.35$, within experimental error. For these samples, then, the shifting and relaxation mechanisms seem to be the same, and the origin of the hyperfine field probably lies in the polarization of ^{23}Na core orbitals by ^{183}W $5d$ conduction-electron orbitals, as for the high- x alloys.^{6,7}

(iii) The structure of Na_xWO_3 throughout the range of x studies is such that room-temperature x-ray powder runs indicate a pure cubic structure, while the NMR shows considerable evidence of distortion. Apparently the crystals are pseudocubic, with the dominant tungsten x-ray scattering centers arranged in a cubic array, but with only about one sodium site in three or four having a cubic close-neighbor environment. Whether the noncubic symmetry is generated by displacement of the oxygen atoms or by off-center occupancy by sodium atoms within the tungsten cube is not clear. Decreasing x generates an increasing quadrupole interaction at the distorted sites, as shown up by the results in column 4, Table III.

(iv) The relaxation rate $(T_1T)^{-1}$ is proportional to x^2 , for $x \geq 0.35$. The peculiar linearity in the dependence of the density of states $g(E_F)$ on x in the sodium tungsten bronzes is therefore confirmed by this relaxation data [since one-electron theory predicts $(T_1T)^{-1} \propto g^2$]. Figure 2 extends this point to the relaxation of the ^{183}W nuclei.

The fact that $(T_1T)^{-1} \propto x^2$ for $x \geq 0.35$ for our measurements is in disagreement with previously published data⁶ on ^{23}Na T_1 's in Na_xWO_3 at low temperatures. However, there is evidence that our samples are less affected by unwanted paramagnetic centers. Also, the ^{183}W results (Fig. 3) are consistent with our ^{23}Na results for $x \geq 0.35$.

(v) For $x \leq 0.35$, $(T_1T)^{-1}$ enhancements appear; in the same range the Knight shift shows little change. This range of alloys is then characterized by much smaller Korringa products, up to two orders of magnitude smaller than the standard metal-like value.

Dealing first with the structural aspects of this investigation, an obvious point can be made about the existence of two inequivalent sodium sites and the consequent splitting of the nuclear-resonance

response into FID and ECHO. The neutron-diffraction data of Atoji and Rundle³¹ point up the existence of two inequivalent sodium sites in an octupled (in volume) unit cell. Using sodium sites at cube corners, tungsten at body centers, and oxygen at face centers, they point out that in the unit cell (containing eight formula units) at $x = 0.75$ two of the eight sodium sites are vacant, the $(0, 0, 0)$ and $(\frac{1}{2}, \frac{1}{2}, \frac{1}{2})$ sites. In addition, to generate the lattice constant doubling, the oxygen atoms are displaced from face-centered positions $(\frac{1}{4}, \frac{1}{4}, 0)$. One may speculate that, for alloys of lower x , the two types of sodium sites are populated randomly, but the $(0, 0, 0)$ and $(\frac{1}{2}, \frac{1}{2}, \frac{1}{2})$ sites retain a cubic nearest-neighbor oxygen configuration, and so give the FID, while the six $(\frac{1}{2}, \frac{1}{2}, 0)$ and $(\frac{1}{2}, 0, 0)$ sites retain a noncubic configuration and so give rise to the ECHO. (The tungsten atoms do not move from their body-centered positions, so that the cubic x-ray data with reduced lattice constant are consistent with this speculation.) If the assumption is made that the ECHO intensity includes no satellite contributions, while the FID intensity includes satellites, then an estimate of the relative numbers of sodium nuclei contributing to the two signals can be made. If an average of column 6, Table III, of 45% is taken, then the ratio of sodium nuclei in the FID to those in the ECHO comes out at 0.26. A value which supports the idea that the two types of signal from ^{23}Na originate from random population of the two inequivalent ^{23}Na sites shown by neutron diffraction.

Moving on to the area where the NMR results interact with transport-property measurements, microscopic theories of percolation have been advanced to explain the diminution in Hall mobility as x decreases,^{10,11} and to explain the linear dependence of specific heat and magnetic susceptibility densities of states on x .¹⁰ Within the model the drop in Hall mobility as x decreases in the region of 0.3 to 0.2¹¹ corresponds to a falloff in the probability that particular conducting channels will stretch unbroken from one end of a crystal to the other.

Above $x = 0.35$, the results here indicate that $(T_1T)^{-1}$ is proportional to x^2 , for both the sodium (Fig. 2) and tungsten nuclei (Fig. 3). For a homogeneous metal, theory predicts $(T_1T)^{-1} \propto g^2(E_F)$ is the density of states per unit volume at the Fermi surface. Thus, if Na_xWO_3 is a homogeneous metal, $g(E_F)$ must be proportional to x ; the fact that susceptibility and specific-heat measurements¹⁶⁻¹⁸ also show $g(E_F) \propto x$ must be accounted as powerful support for the premise, i. e., Na_xWO_3 is a homogeneous metal. The idea¹⁰ that inhomogeneities are the cause of the linear dependence of γ , the specific-heat coefficient, and χ , the susceptibility, on x must now be discarded. Another way of making this point

is to emphasize that the elementary percolation model based on inhomogeneities¹⁰ predicts a nuclear relaxation rate independent of x .

The microscopic density of states $g(E_F)$ depends linearly on x . A simple explanation for this exists, if we bring in the band-structure calculations.^{4,5} A predominantly t_{2g} conduction band has been calculated for related materials KMoO_3 , ReO_3 , with the striking feature of a sharp peak in the density of states of the overlapping bands near the center. Taking these calculations over for the bronzes, the sodium electrons only fill the band one-sixth full even at $\text{Na}_{1.0}\text{WO}_3$, so that the density of states of the conduction band throughout the whole range of the sodium tungsten bronzes is a sharply rising function of energy, i. e., sodium bronzes always have a Fermi level below the peak.

At zero temperature then, a number N of electrons is contained within this band up to level E_F , where

$$N = \int_0^{E_F} g(E) dE.$$

If $g(E)$ has an exponential dependence on energy over the small range involved with sodium-donated electrons, and if $g(0) = 0$, then $N \propto g(E_F) \propto x$.

The very small Korringa products caused by the large enhancement of $(T_1 T)^{-1}$ below $x = 0.35$ could be due to several causes. Specific-heat measurements exclude paramagnetic impurity effects.¹⁸ Leaving aside the technical problems associated with nonexponential relaxation recovery curves, which were discussed in Sec. III, the likeliest causes are either a conversion of conduction-electron wave functions at the Fermi surface from tungsten $5d$ to sodium $3s$ and $3p$ orbitals as x drops below 0.35 or an association between the low mobility observed in this region of concentration with a building up of the spectral density of the electronic magnetic field fluctuations at the Larmor frequency of the sodium nuclei.^{3,32} Since the relaxation rate of nuclear spins can be expressed as the product of a mean square interaction and the spectral density of that interaction at the nuclear resonance frequency, the former possible cause invokes a change of interaction amplitude, the latter a change in the spectral density.

The fluctuation spectrum of electronic magnetic field in ordinary metals is conditioned by the extremely rapid motion at the Fermi surface; the spectral density at the Larmor frequency is therefore low. In low-mobility metals, however, the mean free path L is of the order of an interatomic distance, $k_F L \sim 1$, and conduction becomes diffusive in character. Associated with this change of conduction mechanism the electronic fluctuation spectrum is now conditioned by the much slower diffusive jump time and the spectral density at the

Larmor frequency is enhanced. Warren³ develops a relation between σ and η for this case, where η is defined as the enhancement of the metallic relaxation rate over the value it would have if the electron dynamics were typical of normal metals

$$\sigma\eta = e^2 d^2 / 3\Omega\hbar = \sigma_0, \quad (2)$$

where d is the jump distance and Ω the atomic volume for the electron centers, and σ_0 has a typical value of $3000 (\Omega \text{ cm})^{-1}$. In the bronzes, in the range 0.22–0.35 of interest, this constant term changes at most by 20%, so a direct log-log plot of ρ vs η is useful (Fig. 5), where the line of slope +1 has been superimposed on the data. For the purposes of this figure η was defined as the ratio of the actual rate at 4.2 K, Fig. 2, to the rate which the nuclei would have had if the high-density x^2 proportionality had applied throughout the range of alloys studied. For the 0.30, 0.25, and 0.22 samples $\rho \propto \eta$, and indeed $\sigma_{0.3} \sim 3000 (\Omega \text{ cm})^{-1}$, the accepted starting point below which diffusive conduction starts. (As mentioned earlier, however, the $x = 0.22$ sample may not be metallic.) There is one disquieting feature: the enhancements are much too big at a given conductivity for the constant on the right-hand side of Eq. (2). Within the confines of the model leading to Eq. (2) the discrepancy implies jump distances d approximately five times the expected distance.

The second possible cause for the $(T_1 T)^{-1}$ enhancements at small x could apply if the Na^+ levels

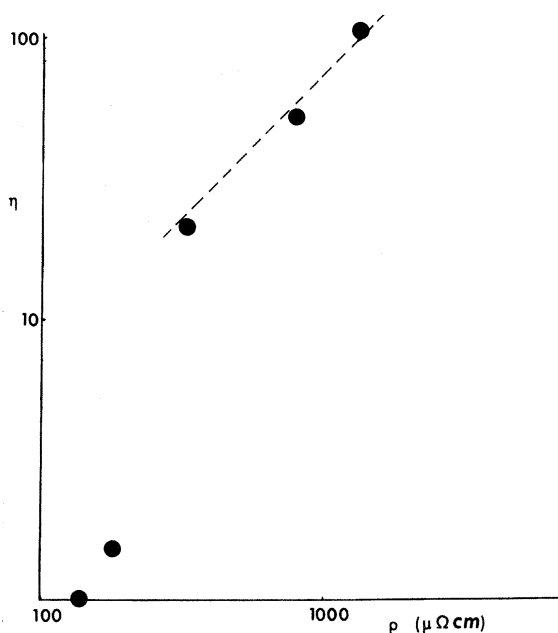


FIG. 5. Graph of η , where η is the relaxation-rate enhancement for Na^{23} defined in the text, against ρ , where ρ is the resistivity of the samples at 300 K; both abscissa and ordinate are logarithmic scales.

lie close to the bottom of the tungsten conduction band. As x decreases, the lattice contracts; this contraction could drive a relative displacement of the Na 3s, 3p, and W 5d bands. The sodium bands, initially at high x lying well above E_F , may be swept down by the lattice contraction to start overlapping the filled portion of the t_{2g} band at about $x=0.30$. Conduction electrons with sodium character have much larger hyperfine fields at sodium nuclei, so relaxation is enhanced. At the same time one may speculate that the Knight shift may acquire cancelling positive and negative (core polarization) contributions from the 3s and 3p functions, respectively. This model for the low- x bronzes compares them in their Knight shift and $(T_1T)^{-1}$ properties to some ordinary metals and alloys such as, for example, the rhodium resonance in Rh_xPd_{1-x} alloys,³³ where for $x \sim 0.70$ the Knight shift is zero while $(T_1T)^{-1}$ remains large. Another example is the ¹⁸³W resonance in high- x bronzes,⁷ where K^2T_1T is much smaller than the theoretical value.

Some approximate calculations can be done to fill out the above suggestion. An example of a metal where the conduction-electron wave functions at the Fermi surface have predominantly s-like character and with a similar density of states at the Fermi level is provided by sodium metal itself. Here $T_1T \sim 5$ sec K, while the 0.25 sample has a $T_1T \sim 15$ min K. Thus 6% s character in the bronzes would produce a $T_1T \sim 23$ min K; the addition of, say, 15% p character might provide a cancelling Knight shift and a further relaxation mechanism, sufficient for the combined relaxation rate to be 15 min K. This particular model therefore entails a 20% change in the character of the wave functions at the Fermi surface as x drops down from 0.35 to 0.25.

It is difficult to choose between these two competing explanations for the sharp rise in $(T_1T)^{-1}$ in low- x sodium-tungsten bronzes; clearly, however, the tungsten relaxation response in these samples will be quite different for the two mechanisms. The recent data of Weinberger,²³ Fig. 3, indicate that the band-crossing mechanism must be preferred. (However, so far these ¹⁸³W measurements have only been taken at one temperature.²³)

These quenched metastable samples of the bronzes appear to be homogeneous low-mobility metals in the concentrations studied, except for $x=0.22$. The specific-heat data,¹⁸ the Hall effect (temperature independent, $R=R_{\text{free electron}}$), and the Knight shift (Table II) all indicate that the properties of the low- x bronzes are similar *mutatis mutandis* to the high- x alloys. Real pseudogap effects, which appear to drive the transition in Ga₂Te₃,³ lead to large differences between R and

$R_{\text{free electron}}$ and to correlations between the Knight shift and conductivity, and so are not present in the low- x bronzes. Effective-medium theories in the dilute regime³⁴ also predict $R > R_{\text{free electron}}$ and would clearly have difficulty explaining the relaxation-rate enhancements. Electron-electron interactions and a Mott-Hubbard gap, and/or band crossing caused by lattice contraction, are possible driving mechanisms.

There remains a basic difficulty in understanding the comparison of the transport properties of general ABO₃ compounds, in particular, strontium titanate SrTiO₃ and potassium tantalate KTaO₃ on the one hand and sodium tungsten bronze Na_xWO₃ on the other; the static dielectric constants of all three are very large, and donor centers in the first two overlap sufficiently to form a metallic impurity band, as in Si:P, at doping densities of about 1 ppm. In Na_xWO₃, however, metallic properties only appear above $x \approx 0.20$. It may be that the A-metal ion plays a more active role in SrTiO₃ and KTaO₃. This statement is supported by work on the ⁸⁷Sr spin-lattice relaxation in SrTiO₃, where, above the purely structural phase transition at 105.5 K, an efficient metallic relaxation mechanism is observed.³⁵ This implies that the impurity-band wave functions at the Fermi surface have considerable interaction with the strontium nuclei.

The transition in the bronzes appears to have similarities to that occurring in^{14,36} Si:P and³⁷ Ge:Sb and to that in³⁸ La_{1-x}Sr_xVO₃; these systems show the same type of rapid decrease in metallic conductivity as the doping level reduces to some critical value, and they may show Anderson localization.³⁹

V. CONCLUSIONS

In the particular phase studied, the tungsten bronzes are only pseudocubic at low temperature. About one in four sodium nuclei remains in a roughly cubic environment throughout the range, and the partitioning of sodium sites occurs most easily via a doubling of the unit cell dimension. Inhomogeneity theories apparently do not explain the transport, specific-heat, and NMR data.

This study confirms the absence of sodium orbital character in the wave functions at the Fermi surface in high- x alloys. However, the Fermi-surface wave function apparently either acquires a small amount of sodium 3s and 3p character as x decreases into the strong-scattering low-mobility region or becomes more effective in relaxing sodium nuclei when the diffusive conduction regime commences.

An interpretation of the linear dependence of the density of the states on x is advanced, requiring that the overlapping t_{2g} conduction bands have an exponential dependence of density of states on ener-

gy over a short range. This requirement is supported by recent band-structure calculations.

ACKNOWLEDGMENTS

I am indebted to Professor D. F. Holcomb for

many lively discussions and practical help throughout this work. I thank the Science Research Council for providing some support and I also thank Cornell University for hospitality during my ten-month stay.

†Work supported in part by the National Science Foundation under Grant No. GH 32250.

*Work done while on leave from the School of Physical Sciences, University of St. Andrews, St. Andrews, Scotland, KY16 9SS.

¹G. Bonera, F. Borsa, M. L. Crippa, and A. Rigamonti, *Phys. Rev. B* **4**, 52 (1971).

²P. A. Lightsey, thesis (Cornell University, 1972) (unpublished).

³W. W. Warren, *Phys. Rev. B* **3**, 3708 (1971).

⁴L. F. Mattheiss, *Phys. Rev. B* **6**, 4718 (1972).

⁵L. F. Mattheiss, *Phys. Rev. B* **2**, 3918 (1970).

⁶A. T. Fromhold and A. Narath, *Phys. Rev.* **136**, A487 (1964).

⁷A. T. Fromhold and A. Narath, *Phys. Rev.* **152**, 585 (1966).

⁸T. Hirose, I. Kawano, and M. Niino, *J. Phys. Soc. Jpn.* **33**, 272 (1972).

⁹B. I. Crowder and M. J. Sienko, *J. Chem. Phys.* **38**, 1576 (1963).

¹⁰R. Fuchs, *J. Chem. Phys.* **42**, 3781 (1965).

¹¹P. A. Lightsey, *Phys. Rev. B* **8**, 3586 (1973).

¹²N. F. Mott, *Electronic Processes in Non-Crystalline Materials* (Clarendon Press, Oxford, 1971).

¹³W. McNeill and L. E. Conroy, *J. Chem. Phys.* **36**, 87 (1962).

¹⁴C. Yamanouchi, K. Mizuguchi, and W. Sasaki, *J. Phys. Soc. Jpn.* **22**, 859 (1967).

¹⁵W. H. Jones, E. A. Garbaty, and R. G. Barnes, *J. Chem. Phys.* **36**, 494 (1962).

¹⁶R. W. Vest, M. Griffel, and J. W. Smith, *J. Chem. Phys.* **28**, 293 (1958).

¹⁷J. D. Greiner, H. R. Shanks, and D. C. Wallace, *J. Chem. Phys.* **36**, 772 (1962).

¹⁸R. Zumsteg (unpublished).

¹⁹M. E. Straumanis, *J. Am. Chem. Soc.* **71**, 679 (1949).

²⁰B. Matthias, *Science* **113**, 591 (1951).

²¹D. Lilienfeld kindly produced these blocks for this work.

²²E. R. Andrew and D. P. Tunstall, *Proc. Phys. Soc. Lond.* **78**, 1 (1961).

²³B. R. Weinberger, M. S. thesis (Cornell University, 1974) (unpublished).

²⁴Thanks to Professor J. H. Freed for giving access to this spectrometer.

²⁵W. G. Clark, *Rev. Sci. Instrum.* **35**, 316 (1964).

²⁶C. Ryter, *Phys. Lett.* **4**, 69 (1963).

²⁷N. Bloembergen and T. J. Rowland, *Acta Metall.* **1**, 731 (1953).

²⁸C. Kittel and E. Abrahams, *Phys. Rev.* **90**, 238 (1953).

²⁹A. Abragam, *The Principles of Nuclear Magnetism* (Clarendon Press, Oxford, 1961), pp. 128ff.

³⁰J. Korringa, *Physica* **16**, 601 (1950).

³¹M. Atoji and R. E. Rundle, *J. Chem. Phys.* **32**, 627 (1960).

³²D. Brown, D. S. Moore, and E. F. W. Seymour, *Philos. Mag.* **23**, 1249 (1971).

³³A. Narath and H. T. Weaver, *J. Appl. Phys.* **41**, 1077 (1970).

³⁴M. H. Cohen and J. Jortner, *Phys. Rev. Lett.* **30**, 699 (1973).

³⁵G. Angelini, G. Bonera, and A. Rigamonti, *Magnetic Resonance and Related Phenomena, Proceedings of the Seventeenth Ampere Congress*, edited by V. Hovi (North-Holland, Amsterdam, 1973), p. 346.

³⁶R. K. Sundfors and D. F. Holcomb, *Phys. Rev.* **136**, A810 (1964).

³⁷F. R. Allen and C. J. Adkins, *Philos. Mag.* **26**, 1027 (1972).

³⁸P. Dougier and A. Casalot, *J. Solid State Chem.* **2**, 396 (1970).

³⁹D. P. Tunstall, *Magnetic Resonance and Related Phenomena, Proceedings of the Eighteenth Ampere Congress*, edited by P. S. Allen, E. R. Andrew, and C. A. Bates (Nottingham Ampere Committee, Department of Physics, Nottingham University, Nottingham, 1974), p. 333.